Discontinuous Galerkin finite element method applied to the coupled Navier-Stokes/Cahn-Hilliard equations

Franck Pigeonneau[1] **and Pierre Saramito**[2]

[1]*Surface du Verre et Interfaces, UMR 125 CNRS/Saint-Gobain*
39, quai Lucien Lefranc - BP 135, 93303 Aubervilliers cedex, France
Franck.Pigeonneau@saint-gobain.com

[2]*Laboratoire Jean Kuntzman*
51, rue des mathématiques BP 53 - Domaine Universitaire, 38041 Grenoble Cedex 9, France
Pierre.Saramito@imag.fr

Abstract

Two-phase flows driven by the interfacial dynamics is studied with a phase-field model to tract implicitly interfaces. The phase field obeys the Cahn-Hilliard equation. The fluid dynamics is described with the Stokes equations with an additional source term in the momentum equation taking into account the capillary forces. A discontinuous Galerkin finite element method is used to solve the coupled Stokes/Cahn-Hilliard equations. The Cahn-Hilliard equation is treated as a system of two coupled equations corresponding to the advection-diffusion equation for the phase field and a non-linear elliptic equation for the chemical potential. First, the variational formulation of the Cahn-Hilliard equation is presented. A numerical test is achieved showing the optimal-order in error bounds. Second, the variational formulation in discontinuous Galerkin finite element approach of the Stokes equations is recalled in which the same space of approximation is used for the velocity and the pressure with an adequate stabilization technique. Finally, numerical simulations describing the capillary rising in a tube is presented.

Keywords: two-phase flows, Cahn-Hilliard equation, phase-field theory, discontinuous Galerkin finite element

1. Introduction

The dynamics of two-phase flows driven by the capillary forces can be adressed by various numerical methods which can be sorted as a function of the method to track interfaces. A first class of methods tracks interfaces explicitly using boundary integral method in the limit of vanishing Reynolds number [13, 12] or front tracking method [20]. This approach is based on the Lagrangian description of interfaces. Despite of the high level of accuracy which can be reached by these techniques, the topological changes are difficult to take into account. A second class of methods tracks interfaces implicitly with a volume indicator like the "Volume of Fluid" technique initially developed by Hirt and Nichols [8] or by a "level-set" method [15, 16]. They are based on the Eulerian description and can straightforward describe topological changes like coalescence or break-up of bubbles or drops. In the two previous approaches, interfaces are considered as a sharp-interfaces without volume. An alternative method considers interface with a small thickness. This technique employs the concept of "phase-field" introduced initially in statistical physics to describe phase change or spinodal decomposition [3]. The development of the phase-field method in fluid mechanics has been summarized by Anderson et al. [2]. This technique is particularly well-adapted to study local effects like triple line dynamics [10] or more recently in [21] or coalescence of drops [22]. Despite of many contributions, find a numerical method to solve efficiently the coupled equations of phase-field model and Navier-Stokes equations is still a research topic in numerical analysis.

In this present work, and since the phase-field method is devoted to study the fluid dynamics at small scale, the fluid inertia can be neglected. Consequently, we investigate the numerical method to solve the coupled Stokes/Cahn-Hilliard equations with a discontinuous Galerkin finite element technique. We start by the problem statement in section 2 in which the Navier-Stokes/Cahn-Hilliard equations will be recalled. The numerical method to solve only the phase-field will be presented in section 3 with a test to determine the numerical errors. Section 4 is devoted to the numerical method of the coupled Stokes/Cahn-Hilliard equations with an example of numerical simulation of a capillary rising.

2. Two-phase flows modelling with a phase-field formulation

We consider a domain $\Omega \subset \mathbb{R}^d$ (with $d = 2$ or 3) in which two fluids are present characterized by the density ρ_1 and the dynamic viscosity η_1 for the fluid 1 and by the density ρ_2 and the dynamic viscosity η_2 for the fluid 2. The fluid phase at any material point with a position $\boldsymbol{x}$ and at each time t is described by an "order parameter" $\phi(\boldsymbol{x}, t)$. By convention, the fluid 1 is given by the order parameter $\phi = 1$ and the fluid 2 by $\phi = -1$. The function ϕ can be seen as a volume fraction.

The phase field method considers that the shift between the two phases occurs over a thin layer equal to ζ corresponding to the "diffuse interface" thickness. Under the actions of external forces, boundary conditions and interaction between the two phases, the media changes in space and time requiring balance equations. Moreover, the dynamics between the two phases has to be considered by writing an equation on the phase field ϕ.

The phase-field model applied for binary fluid is designated as the "model H" by Hohenberg and Halperin [9]. The details of the derivation of the Navier-Stokes/Cahn-Hilliard equations are not provided in this article. For more information, reader can read references [2]. In the following, the Navier-Stokes/Cahn-Hilliard equations are written under dimensionless form with a characteristic length L, velocity U, viscosity η_1 and density ρ_1 which will be provided in the numerical examples presented in section 4. In the following, we assume that the fluid is incompressible. The gravity force is taken into account with a direction given by a unit

vector $\boldsymbol{g}$ normalized by the magnitude of the gravity acceleration, g. The coupled system of equations is given by

$$\begin{aligned}
\operatorname{div} \boldsymbol{u} &= 0, && (1)\\
\operatorname{Re} \rho(\phi) \frac{D\boldsymbol{u}}{Dt} &= -\boldsymbol{\nabla} P + \operatorname{div}\left[2\eta(\phi)\boldsymbol{D}(\boldsymbol{u})\right] + \\
&\quad \frac{\operatorname{Bo}}{\operatorname{Ca}} \rho(\phi)\boldsymbol{g} + \frac{3}{2\sqrt{2}\operatorname{Ca}\operatorname{Cn}} \mu \boldsymbol{\nabla}\phi, && (2)\\
\frac{D\phi}{Dt} &= \frac{1}{\operatorname{Pe}} \boldsymbol{\nabla}^2 \mu(\phi), && (3)\\
\mu(\phi) &= \phi(\phi^2 - 1) - \operatorname{Cn}^2 \boldsymbol{\nabla}^2 \phi, && (4)
\end{aligned}$$

in which the two first equations are the Navier-Stokes equations with $\boldsymbol{D}$ the rate-of-strain tensor and the two lasts are the Cahn-Hilliard equation. The coupling between the phase-field is achieved by the capillary force given by the last term of the right-hand side of the momentum equation, eq. (2) and also by the chance of the density and viscosity as function of ϕ. The Cahn-Hilliard equation has been written in two parts in order to have two equations at the second order useful for the numerical methods which are presented below. The last equation defines the chemical potential in which the first term is the derivative respect to ϕ of the double-well potential admitting two local minima in $\phi = \pm 1$ and the second term takes into account the energy due to interface. At the equilibrium, the chemical potential must be equal to zero. Seven dimensionless numbers arise in the problem for which the first six numbers are defined by

$$\operatorname{Re} = \frac{\rho_1 U L}{\eta_1},\ \operatorname{Bo} = \frac{\rho_1 g L^2}{\sigma},\ \operatorname{Ca} = \frac{\eta_1 U}{\sigma}, \quad (5)$$

$$\operatorname{Cn} = \frac{\zeta}{L},\ \hat{\rho} = \frac{\rho_2}{\rho_1},\ \hat{\eta} = \frac{\eta_2}{\eta_1}. \quad (6)$$

The first one is the so-called Reynolds number which will be assumed much lesser than one in the following in order to neglect the fluid inertia. The Bond number Bo measures the ratio of gravity to surface tension forces characterized by the surface tension σ while the capillary number Ca compares the viscosity effect to the surface tension one. The Cahn number Cn is the ratio of the diffuse-interface thickness ζ to the length scale. The seventh dimensionless number Pe given without definition is the Péclet number comparing the diffusion time scale of the chemical potential to the convective time scale which is always greater than one. The normalized density and dynamic viscosity are given by an arithmetic average:

$$\rho(\phi) = \frac{1+\hat{\rho}}{2} + \frac{1-\hat{\rho}}{2}\phi, \quad (7)$$

$$\eta(\phi) = \frac{1+\hat{\eta}}{2} + \frac{1-\hat{\eta}}{2}\phi. \quad (8)$$

Initial and boundary conditions will be provided in the following when the numerical method will be presented.

3. Numerical resolution of Cahn-Hilliard equation

We start by the presentation of the numerical method to solve the Cahn-Hilliard equation with a discontinuous Galerkin finite element method. Clearly, the Cahn-Hilliard equation is a nonlinear fourth-order partial differential equation needing a high level of regularity. The application of discontinuous Galerkin method to solve the phase-field model has been initiated by Feng and Karakashian [7] among others. They established an optimal-order error bound by solving the fourth-order equation when the polynomial degree is greater or equal to two. Here, according the previous work of Kay et al. [11], the problem is set as a system of two second-order elliptic equations. In this section, the solenoidal velocity field $\boldsymbol{u}$ is assumed known.

3.1. Discontinuous Galerkin finite element formulation

The continuous problem is

Problem 1 (Cahn-Hilliard problem) *find $\phi(\boldsymbol{x},t)$ and $\mu(\boldsymbol{x},t)$ defined in $\Omega \times [0,T]$ such as*

$$\begin{aligned}
\frac{\partial \phi}{\partial t} + \boldsymbol{u}\cdot\boldsymbol{\nabla}\phi - \frac{1}{\operatorname{Pe}}\boldsymbol{\nabla}^2\mu(\phi) = 0,\ \textit{in } \Omega\times[0,T], && (9)\\
-\mu(\phi) + \phi(\phi^2-1) - \operatorname{Cn}^2\boldsymbol{\nabla}^2\phi = 0,\ \textit{in } \Omega\times[0,T], && (10)\\
\phi(\boldsymbol{x}, t=0) = \phi_0(\boldsymbol{x}),\ \textit{in } \Omega, && (11)\\
\frac{\partial \phi}{\partial n} = f(\phi),\ \textit{on } \partial\Omega, && (12)\\
\frac{\partial \mu}{\partial n} = 0,\ \textit{on } \partial\Omega. && (13)
\end{aligned}$$

Moreover, the normal component of the velocity $\boldsymbol{u}\cdot\boldsymbol{n}$ is equal to zero on $\partial\Omega$ for $\boldsymbol{n}$ the exterior unit normal on $\partial\Omega$. The boundary condition on ϕ, eq. (12), has been taken in general form because in applications, the interaction with a wall for instance involves a condition on normal derivative of ϕ to impose a certain contact angle [10, 21].

To solve numerically this problem, a discontinuous Galerkin method initially developed by Kay et al. [11] has been chosen. The main property of the formulation is the optimal-order in error bounds as it will be verified below for a polynomial degree greater or equal to one.

Let $\mathcal{T}_h$ be a triangulation of the domain Ω formed by finite elements K with meshsize $h = \operatorname{diam}(K)$ such as $\mathcal{T}_h = \{K\}$ and $\overline{\Omega} = \bigcup_{K\in\mathcal{T}_h} \overline{K}$. Furthermore, we consider a subset of faces F formed by interfaces between two distint mesh elements K_+ and K_- such as $F = \partial K_- \cap \partial K_+$ and boundary faces given by $F = \partial K \cap \partial\Omega$. For internal face, orientation has to be precised. The unit normal $\boldsymbol{n}_F$ is outward of K_- and inward of K_+. If $\mathcal{F}_h^i$ gathers all interfaces and $\mathcal{F}_h^b$ all boundary faces, the set of faces is $\mathcal{F}_h = \mathcal{F}_h^i \cup \mathcal{F}_h^b$. Finally, the local length scale at the face F noted h_F is defined according to Di Pietro and Ern [6], chap. 4 page 125.

In the below formulation, some usual notations in the context of the discontinuous Galerkin method have to be precised. First, since for all $\phi_h \in X_h$ is discontinuous, the broken gradient $\boldsymbol{\nabla}_h$ is defined by [6]

$$\left(\boldsymbol{\nabla}_h \phi_h\right)_{|K} = \boldsymbol{\nabla}\left(\phi_{h|K}\right),\ \forall\, K \in \mathcal{T}_h. \quad (14)$$

Moreover, at each interior face F, let define $\phi_h^- = \phi_{h|K_-}$ the inner value and $\phi_h^+ = \phi_{h|K_+}$ the outer value. We define the jump by $[\![\phi_h]\!] = \phi_h^- - \phi_h^+$ and the average $\{\!\{\phi_h\}\!\} = (\phi_h^- + \phi_h^+)/2$.

The discontinuous finite element space is defined by

$$X_h = \{v_h \in L^2(\Omega);\ v_{h|K} \in P_k,\ \forall\, K \in \mathcal{T}_h\}, \quad (15)$$

with k the polynomial degree. This space belongs to the broken Sobolev space

$$H^1(\mathcal{T}_h) = \{v \in L^2(\Omega);\ v_{|K} \in H^1(K),\ \forall\, K \in \mathcal{T}_h\}. \quad (16)$$

The variational formulation of the Cahn-Hilliard problem takes the following form

Problem 2 *Find ϕ_h, $\mu_h \in X_h$ such that*

$$\begin{aligned}
\operatorname{Pe}^{-1} a(w_h, \mu_h) + b(w_h, \phi_h) = 0,\ \textit{for } w_h \in X_h, && (17)\\
-(q_h, \mu_h) + (q_h, \phi_h^3 - \phi_h) + \operatorname{Cn}^2 a(q_h, \phi_h) = \\
l(q_h, \phi_h),\ \textit{for } q_h \in X_h, && (18)
\end{aligned}$$

in which

$$a(w_h, \mu_h) = \int_\Omega \boldsymbol{\nabla}_h w_h \cdot \boldsymbol{\nabla}_h \phi_h dV -$$

$$\sum_{F\in\mathcal{F}_h^i} \int_F \left[\{\!\{\boldsymbol{\nabla}\mu_h\cdot\boldsymbol{n}_F\}\!\}[\![w_h]\!] + \{\!\{\boldsymbol{\nabla}w_h\cdot\boldsymbol{n}_F\}\!\}[\![\mu_h]\!] - c_F[\![\mu_h]\!][\![w_h]\!]\right] dS, \quad (19)$$

$$b(w_h,\phi_h)=\left(\frac{\partial\phi_h}{\partial t},w_h\right)+\int_\Omega \boldsymbol{\nabla}_h\phi_h\cdot\boldsymbol{u}_h w_h dV+ \sum_{F\in\mathcal{F}_h^i}\int_F\left(\frac{1}{2}|\boldsymbol{u}_h\cdot\boldsymbol{n}_F|[\![\phi_h]\!][\![w_h]\!]- \boldsymbol{u}_h\cdot\boldsymbol{n}_F[\![\phi_h]\!]\{\!\{w_h\}\!\}\right)dS, \quad (20)$$

$$l(q_h,\phi_h)=\mathrm{Cn}^2\sum_{F\in\mathcal{F}_h^b}\int_F f_h(\phi_h)q_h dS,\ for\ q_h\in X_h. \quad (21)$$

The details of the derivation of this variational formulation can be found in [11]. The penalty parameter c_F is equal to the product $\beta\varpi_F$ with $\beta=(k+1)(k+d)/d$ (d space dimension) and ϖ_F by [17]

$$\varpi_F=\begin{cases}\frac{\mathrm{meas}(\partial K)}{\mathrm{meas}(K)} & \text{for } F\in K\cap\partial\Omega,\\ \max\left(\frac{\mathrm{meas}(\partial K_+)}{\mathrm{meas}(K_+)},\frac{\mathrm{meas}(\partial K_-)}{\mathrm{meas}(K_-)}\right) & \text{for } F\in K_-\cap K_+.\end{cases} \quad (22)$$

The convective term of the phase-field has been written according to the development of Di Pietro and Ern [6] with an upwinding flux approximation. The main feature of the discontinuous Galerkin method is to have an accurate mass conservation applied to convective equation. This behavior has been controlled carefully in the paper [19] presented in this conference and is not addressed in the present contribution.

For the time discretization, a Backward Differential Formula (BDF) at order $p\leq 6$ is used. If Δt is the time step, the temporal derivative at the time $t=n\Delta t$ of the ϕ_h^n at the order p is given by

$$\frac{\partial\phi_h^n}{\partial t}=\frac{1}{\Delta t}\sum_{l=0}^{p}\alpha_{pl}\phi_h^{n-l}+\mathcal{O}(\Delta t^p), \quad (23)$$

for which coefficients α_{pl} can be found in the book of Süli and Mayers [18] (chap. 12, page 349).

This time derivative obtained by the previous formula is introduced in $b_h(w_h,\phi_h^n)$ leading to a source term obtained with a combination of ϕ_h^{n-l} with $1\leq l\leq p$ following equation (23). Moreover, the non-linearities of the Cahn-Hilliard problem are solved using a Newton algorithm.

3.2. *Numerical tests*

The previous problem has been implemented in the Rheolef C++ finite element library [14]. To test the numerical solver, the numerical experiment proposed by Kay et al. [11] is used for which the Cahn-Hilliard equation is solved with a velocity field given by

$$\boldsymbol{u}=f(r)(y,-x)^T,\ \forall(x,y)\in[-1;1]^2, \quad (24)$$

$$\text{with } f(r)=\frac{1+\tanh[\beta(1-3r)]}{2},\ \text{and } r=\sqrt{x^2+y^2}, \quad (25)$$

in a domain $\Omega=[-1;1]^2$. An exact solution of the phase-field given by

$$\phi_e=t\cos(\pi x)\cos(\pi y),\ \forall(x,y)\in[-1;1]^2 \text{ and } t\in]0;1], \quad (26)$$

is imposed by adding an adequate source term in eq. (9). The range of time is taken in $[0;1]$. The domain has been discretized with a regular triangular elements with 16, 32 and 64 elements over each Cartesian coordinate.

We perform the numerical experiment with Cahn number equal to 10^{-1} and for a Péclet number equal to 50. The temporal numerical scheme at the second order (BDF-2) has been used with a time step equal to 10^{-2}. Three polynomial degrees have been tested with $k=1$, 2 and 3. Errors between the numerical solution and the exact solution have been computed with L^2 and H^1 norms defined as follows

$$||v||_{L^2,h}^2=\int_\Omega v^2 dV, \quad (27)$$

$$||v||_{H^1,h}^2=\int_\Omega \boldsymbol{\nabla}_h v\cdot\boldsymbol{\nabla}_h v dV+\sum_{F\in\mathcal{F}_h}\int_F\varpi_F[\![v]\!]^2 dS. \quad (28)$$

Figures 1 and 2 depict errors integrated over the time range $[0,1]$ as a function of the mesh size both for the phase field and the chemical potential. For each polynomial degree, errors behave as $\mathcal{O}(h^n)$. The exponent n has been provided in Figures 1 and 2 for each polynomial degree. As expected, errors computed in L^2 norm behave approximately as $\mathcal{O}(h^{k+1})$ both for the phase field ϕ and for the chemical potential and as $\mathcal{O}(h^k)$ in H^1 norm showing that the numerical implementation is optimal-order in error bounds.

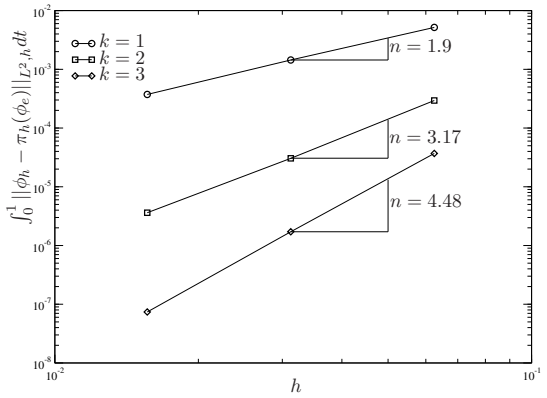

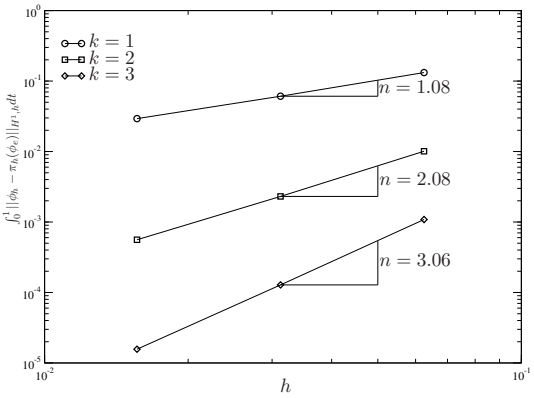

Figure 1: Errors $\int_0^1||\phi_h-\pi_h(\phi_e)||_{L^2,h}dt$ and $\int_0^1||\phi_h-\pi_h(\phi_e)||_{H^1,h}dt$ as a function of mesh size for the three polynomial degrees.

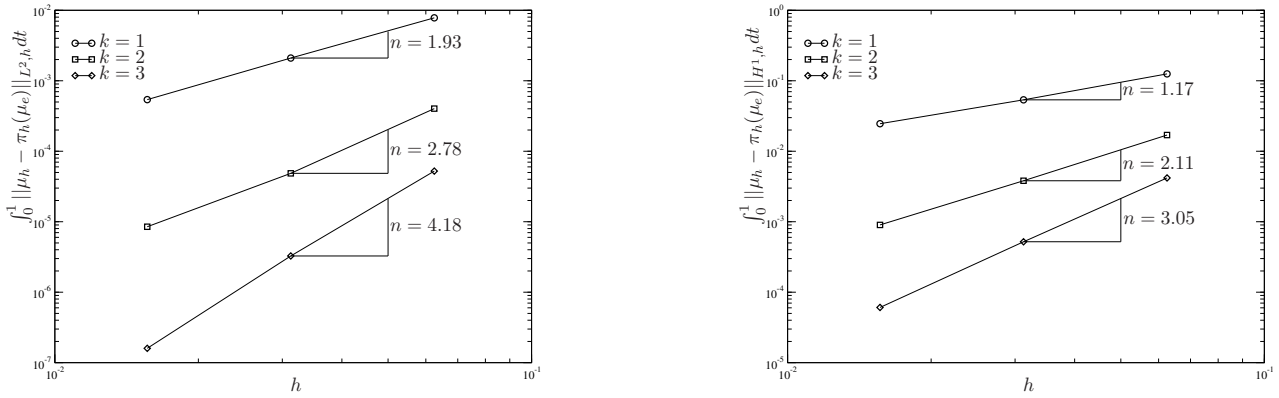

Figure 2: Errors $\int_0^1 ||\mu_h - \pi_h(\mu_e)||_{L^2,h} dt$ and $\int_0^1 ||\mu_h - \pi_h(\mu_e)||_{H^1,h} dt$ as a function of mesh size for the three polynomial degrees.

4. Numerical resolution of Cahn-Hilliard and Stokes equations

We now turn on the numerical resolution of Cahn-Hilliard and Navier-Stokes equations. Here, the Reynolds number is assumed much lesser than one in order to neglect the inertia of the fluid. In this limit, the Navier-Stokes equations are reduced to the Stokes equations. The continuous problem is similar to the set of equations (1-4) given in § 2 in which the inertia term in the momentum equation is removed. Initial and boundary conditions for ϕ and μ can be written in general form as in equations (11-13). In order to take into account the boundary conditions for which velocity or stress are imposed, the frontier of Ω is shared between $\partial\Omega_D$ for which

$$\boldsymbol{u} = \boldsymbol{u}_D, \tag{29}$$

and $\partial\Omega_N$ where

$$\boldsymbol{\sigma}\cdot\boldsymbol{n} = \boldsymbol{t}_N, \tag{30}$$

such as $\partial\Omega_D \cap \partial\Omega_N = \emptyset$ and $\partial\Omega = \partial\Omega_D \cup \partial\Omega_N$. The stress tensor is given by $-P\mathbf{1} + 2\eta(\phi)\boldsymbol{D}(\boldsymbol{u})$ with $\mathbf{1}$ the unit tensor. Boundary faces, $\mathcal{F}_h^b$, are now shared in two sub-sets $\mathcal{F}_h^{b,D}$ and $\mathcal{F}_h^{b,N}$ corresponding to $\partial\Omega_D$ and $\partial\Omega_N$ respectively.

A discontinuous Galerkin finite element method is also used to solve the Stokes equations. As it will be detailed below velocity and pressure are approximated at the same polynomial degree m. So, the discontinuous finite element spaces are defined by

$$\boldsymbol{V}_h = \{\boldsymbol{u}_h \in L^2(\Omega)^d; \boldsymbol{u}_{|K} \in P_m,\ \forall K \in \mathcal{T}_h\}, \tag{31}$$

$$Q_h = \{q_h \in L^2(\Omega); q_{|K} \in P_m,\ \forall K \in \mathcal{T}_h\}. \tag{32}$$

To solve the problem as a function of time, a BDF-p scheme is used to solve the phase-field equation in which the velocity field is extrapolated at the same order that the BDF scheme using the forward difference formula [1]

$$\boldsymbol{u}_h^{*,n} = \sum_{l=1}^{p} \binom{p}{l} (-1)^{l-1} \boldsymbol{u}_h^{n-l} + \mathcal{O}(\Delta t^p). \tag{33}$$

At the time step n, ϕ_h^n and μ_h^n are determined by solving the problem 2 in which the convective equation is solved using $\boldsymbol{u}_h^{*,n}$. Once the phase-field problem is solved, the Stokes equations have to be solved taking into account the capillary source term given by the last term of the right-hand side of (2).

4.1. Discontinuous Galerkin finite element formulation of Stokes problem

Since the Stokes equations are in quasi-steady state, the reference of the time is removed in the following in order to simplify the notation. The variational formulation follows the method initially introduced by Cockburn et al. [4] which has been studied theoretically by Di Pietro and Ern [6]. The heterogeneity of the viscosity needs to generalize the formulation according to the previous developments achieved in heterogeneous diffusion [6] (chap. 4). The discrete variational formulation writes:

Problem 3 (Stokes problem) *find $\boldsymbol{u}_h \in \boldsymbol{V}_h$ and $P_h \in Q_h$ such that*

$$\alpha(\boldsymbol{u}_h, \boldsymbol{v}_h) + \beta(\boldsymbol{v}_h, P_h) = \lambda(\boldsymbol{v}),\ \forall \boldsymbol{v}_h \in \boldsymbol{V}_h, \tag{34}$$

$$\beta(\boldsymbol{u}_h, q_h) - \gamma(p_h, q_h) = 0,\ \forall q_h \in Q_h, \tag{35}$$

with

$$\begin{aligned}\alpha(\boldsymbol{u}_h, \boldsymbol{v}_h) = &\int_\Omega 2\eta \boldsymbol{D}_h(\boldsymbol{u}_h) : \boldsymbol{D}_h(\boldsymbol{v}_h) dV + \\ &\sum_{F\in\mathcal{F}_h^i\cup\mathcal{F}_h^{b,D}} \int_F [c_F\eta_F [\![\boldsymbol{u}]\!]\cdot[\![\boldsymbol{v}]\!] - \\ &\{\!\{2\eta \boldsymbol{D}_h(\boldsymbol{u}_h)\cdot\boldsymbol{n}_F\}\!\}_\omega [\![\boldsymbol{v}_h]\!] - \\ &\{\!\{2\eta \boldsymbol{D}_h(\boldsymbol{v}_h)\cdot\boldsymbol{n}_F\}\!\}_\omega [\![\boldsymbol{u}_h]\!]] \, dS,\end{aligned} \tag{36}$$

$$\begin{aligned}\beta(\boldsymbol{u}_h, q_h) = &-\int_\Omega q_h \boldsymbol{\nabla}_h\cdot\boldsymbol{u}_h dV + \\ &\sum_{F\in\mathcal{F}_h^i} \int_F [\![\boldsymbol{u}]\!]\cdot\boldsymbol{n}_F \{\!\{q_h\}\!\} dS,\end{aligned} \tag{37}$$

$$\begin{aligned}\lambda(\boldsymbol{v}) = &\int_\Omega \left[\frac{\mathrm{Bo}}{\mathrm{Ca}}\rho_h \boldsymbol{g} + \frac{3}{2\sqrt{2}\,\mathrm{Ca}\,\mathrm{Cn}}\right. \\ &\left.\mu_h \boldsymbol{\nabla}_h\phi_h\right]\cdot\boldsymbol{v}_h dV + \\ &\sum_{F\in\mathcal{F}_h^{b,D}} \int_F \boldsymbol{u}_{h,D}\cdot[c_F\boldsymbol{v}_h - 2\eta \boldsymbol{D}_h(\boldsymbol{v}_h)\cdot\boldsymbol{n}] \, dS + \\ &\sum_{F\in\mathcal{F}_h^{b,N}} \int_F \boldsymbol{t}_{h,N}\cdot\boldsymbol{v}_h dS,\end{aligned} \tag{38}$$

$$\gamma(p_h, q_h) = \sum_{F\in\mathcal{F}_h^i} \int_F h_F [\![p_h]\!][\![q_h]\!] dS. \tag{39}$$

The viscosity at the face F and the weighted average $\{\!\{\cdot\}\!\}_\omega$ are defined by [6]

$$\eta_F = \frac{2\eta_h^+\eta_h^-}{\eta_h^+ + \eta_h^-}, \tag{40}$$

$$\{\!\{v_h\}\!\}_\omega = \frac{\eta_h^+ v_h^- + \eta_h^- v_h^+}{\eta_h^+ + \eta_h^-}. \tag{41}$$

Clearly, when the viscosity is constant, the usual arithmetic average is found.

4.2. *Numerical tests: capillary rising*

When a liquid is introduced in a capillary tube with a diameter D, the liquid rises due to the wetting of the liquid on the tube wall. At the equilibrium, the rising height depends on the wetting angle θ, the surface tension σ, the liquid density ρ_1, the gravity and the tube diameter. According to de Gennes et al. [5], the height over which the liquid rises can be written as follows

$$\frac{h_{\text{cap}}}{D} = \frac{4\cos\theta}{\text{Bo}}, \tag{42}$$

in which the Bond number is defined with D as a length scale. When $\theta < \pi/2$ corresponding to "wetting" condition, h_{cap} is positif while if $\theta < \pi/2$ ("non-wetting" condition), h_{cap} is negatif meaning that the liquid goes down occurring for a liquid metal like mercury, for instance.

The dynamics of rising can be studied with the Stokes/Cahn-Hilliard equations for which the wetting condition can be introduced easily. We perform with Rheolef library a numerical simulation in an axisymmetric geometry depicted in Figure 3 corresponding to the one half of the tube. The problem is normalized by a length scale equal to the tube diameter. The velocity scale is taken by writing the balance between gravity and viscous forces meaning that the capillary and Bond numbers become equivalent.

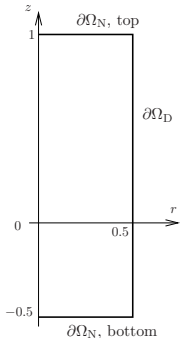

Figure 3: Geometry of a liquid rising in a tube with a radius equal to $1/2$.

In the limit of vanishing Reynolds number, five dimensionless numbers have to be considered. For the phase-field modelling, the physical length scale of interface is around few nanometers meaning that the ratio of this interface thickness and the tube diameter is too small. Fortunately, the "sharp-interface" behavior is obtained for a larger Cahn number [21]. Consequently, in the following, the Cahn number is taken equal to 10^{-2}. The Péclet number has to be taken sufficiently large to limit the diffusion. Here, Pe is set at 10^2. Ratios $\hat{\rho}$ and $\hat{\eta}$ are taken respectively at 10^{-3} and 10^{-2} which are the typical values for water (fluid 1) and air (fluid 2).

The boundary conditions on $\partial\Omega_{\text{D}}$ and $\partial\Omega_{\text{N}}$ depicted in Figure 3 are the following

$$\boldsymbol{u} = 0,\ \frac{\partial\phi}{\partial n} = \frac{(1-\phi^2)\sqrt{2}\cos\theta}{2\,\text{Cn}},\ \frac{\partial\mu}{\partial n} = 0,\ \forall \boldsymbol{x} \in \partial\Omega_{\text{D}}, \tag{43}$$

$$\boldsymbol{\sigma}\cdot\boldsymbol{n} = 0,\ \frac{\partial\phi}{\partial n} = \frac{\partial\mu}{\partial n} = 0,\ \forall \boldsymbol{x} \in \partial\Omega_{\text{N}}, \text{top}, \tag{44}$$

$$\boldsymbol{\sigma}\cdot\boldsymbol{n} = -(\hat{\rho} + \frac{1}{2})\boldsymbol{n},\ \frac{\partial\phi}{\partial n} = \frac{\partial\mu}{\partial n} = 0,\ \forall \boldsymbol{x} \in \partial\Omega_{\text{N}}, \text{bottom}. \tag{45}$$

On $\partial\Omega_{\text{D}}$, the wetting condition has been written according to the previous works of Jacqmin [10] and Yue et al. [21]. Moreover, the non-slip condition is applied on $\partial\Omega_{\text{D}}$. On the top and the bottom of the tube, we apply a pressure with stress free condition. At the bottom, the pressure arises from a simple static equilibrium used as initial condition in order to start from the static condition. Initially, fluid 1 is located below the plane $z = 0$ in such of way that ϕ is given by the exact solution of the Cahn-Hilliard equation in one-dimension:

$$\phi_0(z,r) = -\tanh\left(\frac{z}{\sqrt{2}\,\text{Cn}}\right). \tag{46}$$

Starting with a plane interface, we impose a contact angle equal to $\theta = 17\pi/36$. The numerical simulations have been achieved with BDF-2 and a time step 10^{-2}. Due to the contact angle lesser than $\pi/2$, the fluid interface curves close to the wall leading to a pressure jump. Figure 4 depicts the pressure field for three times equal to 2, 20 and 60. Clearly, at the beginning, the pressure decreases close to the wall due to the curvature and Laplace pressure. Consequently, the liquid goes up. At large time, the pressure obeys at the hydrostatic solution leading to the immobilization of the liquid column.

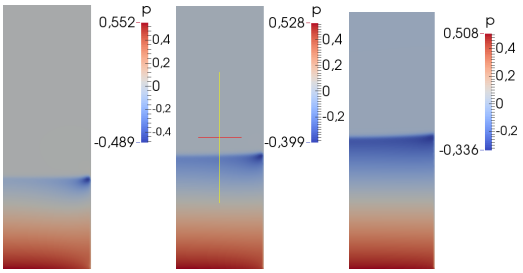

Figure 4: Pressure field in the tube at time $t = 2$, 20 and 60 for a contact angle equal to $17\pi/36$.

Figure 5 presents the superposition of the phase-field and velocity field at $t = 2$, 20 and 60. At the beginning of the rising the velocity is relatively important and decreases when the liquid goes up. When $t = 60$, the magnitude of the velocity is one order of magnitude lesser than the value observed at $t = 2$.

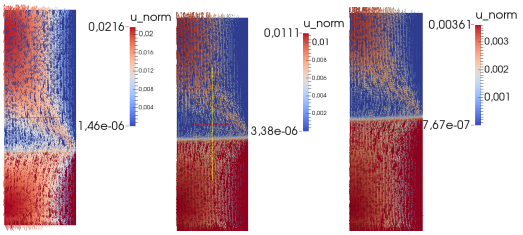

Figure 5: Phase-field and velocity field in the tube at time $t = 2$, 20 and 60 for a contact angle equal to $17\pi/36$.

To follow the rising of the interface, we plot in Figure 6 the position of the triple line z_{TL} as a function of time. An algebraic behavior is clearly established with a slope close to 0.83. The asymptotic hydrostatic equilibrium is very well found numerically since the position of the triple line reaches the level predicted by equation (42).

Pressure P is plotted as a function of z on the symmetric axis when $t = 100$ in Figure 7. The hydrostatic solution in the liquid is very well found. Pressure in the second phase is quasi-uniform since the density of fluid 2 is very small. Moreover, at the interface, the pressure jump due to the interface curvature is around 0.3 while a simple hydrostatic computation gives a value equal to 0.34 on the symmetric axis. Nevertheless, remark that the numerical solution does not reach the asymptotic static state.

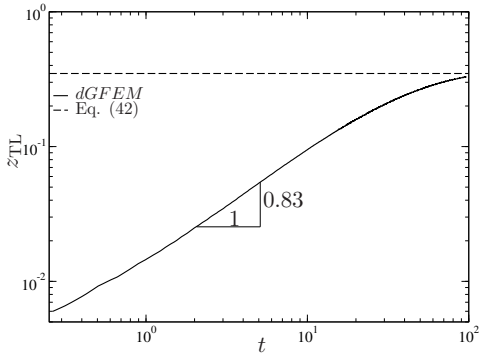

Figure 6: Position of the triple line, z_{TL} as a function of time for a contact angle equal to $17\pi/36$.

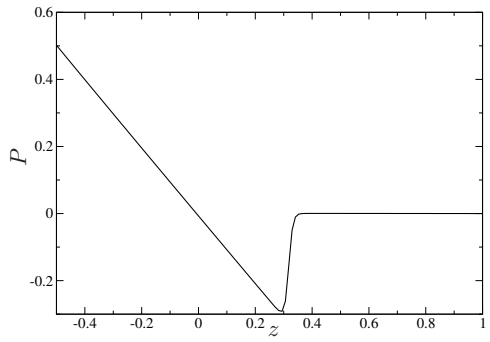

Figure 7: P vs z on the z-axis at $t = 100$ for a contact angle equal to $17\pi/36$.

5. Conclusion

In this contribution, we develop a numerical method to solve the coupled Stokes/Cahn-Hilliard equations with a discontinuous Galerkin finite element method. The scheme on the Cahn-Hilliard is optimal-order in error bounds and this fact has been verified numerically. A numerical method for Stokes/Cahn-Hilliard equations has been also developed for which the Stokes solver with heterogeneous viscosity has been established.

In order to study the dynamics of the triple line physics, we have solved the problem of the capillary rising in a circular tube. The dynamics is very well reproduced and the asymptotic behavior of the static pressure equilibrium is captured.

This first numerical test prove the relevance of this kind of model to describe the dynamics of triple line accurately.

References

[1] M. Abramowitz and I. A. Stegun. *Handbook of mathematical functions*. Dover Publications, Inc., New York, 1965.

[2] D. M. Anderson, G. B. McFadden, and A. A. Wheeler. Diffuse-interface methods in fluid mechanics. *Annu. Rev. Fluid Mech.*, 30:139–165, 1998.

[3] J. W. Cahn and J. E. Hilliard. Free Energy of a Nonuniform System. I. Interfacial Free Energy. *J. Chem. Phys.*, 28(2):258, 1958.

[4] B. Cockburn, G. Kanschat, D. Schötzau, and C. Schwab. Local discontinuous galerkin methods for the stokes system. *SIAM J. Numer. Anal.*, 40(1):319–342, 2002.

[5] P.-G. de Gennes, F. Brochard-Wyart, and D. Quéré. *Gouttes, bulles, perles et ondes*. Belin, Paris, 2005.

[6] D. A. Di Pietro and A. Ern. *Mathematical aspects of discontinuous Galerkin methods*. Springer-Verlag, Heidelberg, 2012.

[7] X. Feng and O. A. Karakashian. Fully discrete dynamic mesh discontinuous galerkin methods for the cahn-hilliard equation of phase transition. *Math. Comp.*, 76:1093–1117, 2007.

[8] C. W. Hirt and B. D. Nichols. Volume of fluid (VOF) method for the dynamics of free boundaries. *J. Comput. Phys.*, 39:201–226, 1981.

[9] P. C. Hohenberg and B. I. Halperin. Theory of dynamic critical phenomena. *Rev. Mod. Phys.*, 49(3):435–479, 1977.

[10] D. Jacqmin. Contact-line dynamics of a diffuse fluid interface. *J. Fluid Mech.*, 402:57–88, 2000.

[11] D. Kay, V. Styles, and E. Süli. Discontinuous Galerkin finite element approximation of the Cahn-Hilliard equation with convection. *SIAM J. Numer. Anal.*, 47(4):2660–2685, 2009.

[12] F. Pigeonneau and A. Sellier. Low-Reynolds-Number gravity-driven migration and deformation of bubbles near a free surface. *Phys. Fluids*, 23:092102, 2011.

[13] C. Pozrikidis. *Boundary integral and singularity methods for linearized viscous flow*. Cambridge University Press, Cambridge, 1992.

[14] P. Saramito. *Efficient C++ finite element computing with Rheolef: vol. 2. Discontinuous Galerkin methods*. CNRS-CCSD ed., 2015.

[15] J. A. Sethian. *Level set methods and fast marching methods. Evolving interfaces in computational geometry, fluid mechanics, computer vision, and materials science*. Cambridge University Press, Cambridge, 1999.

[16] J. A. Sethian and P. Smereka. Level set methods for fluid interfaces. *Annu. Rev. Fluid Mech.*, 35:341–371, 2003.

[17] K. Shahbazi. An explicit expression for the penalty parameter of the interior penalty method. *J. Comput. Phys.*, 205(2):401–407, 2005.

[18] E. Süli and D. F. Mayers. *An Introduction to Numerical Analysis*. Cambridge University Press, Cambridge (UK), 2003.

[19] M. Ta, F. Pigeonneau, and P. Saramito. An implicit high order discontinuous galerkin level set method for two-phase flow problems. In *ICMF-2016 - 9th International Conference on Multiphase Flow*, pages 1–6, Firenze, Italy, May 22nd-27th 2016.

[20] A. O. Unverdi and G. Tryggvason. A front-tracking method for viscous, incompressible, multi-fluid flows. *J. Comput. Phys.*, 100:25–37, 1992.

[21] P. Yue, C. Zhou, and J. J. Feng. Sharp-interface limit of the Cahn-Hilliard model for moving contact lines. *J. Fluid Mech.*, 645:279, 2010.

[22] Pengtao Yue, James J. Feng, Chun Liu, and Jie Shen. Diffuse-interface simulations of drop coalescence and retraction in viscoelastic fluids. *J. Non-Newtonian Fluid Mech.*, 129(3):163–176, 2005.